Acoustic Attenuation Characteristics of Surface-Modified Polymeric Porous Microspheres

Yeap-Hung Ng, Liang Hong

Department of Chemical and Biomolecular Engineering, National University of Singapore, Singapore 119260

Received 5 January 2006; accepted 27 February 2006
DOI 10.1002/app.24418
Published online in Wiley InterScience (www.interscience.wiley.com).

ABSTRACT: Porous microspheres (30–50 μm) of poly (styrene-*co*-divinylbenzene) (SD), poly(styrene-*co*-2-hydroxyethyl acrylate-*co*-divinylbenzene) (SDH), and poly(methyl acrylate-*co*-divinylbenzene) (MD) have been synthesized as the basic unit of acoustic shielding medium. To improve their acoustic insulating property, the structural modifications involving deposition of Ni particles ($d < 100$ nm) by *in situ* reduction or electroless plating and incorporation of soft poly(ethyl acrylate) chains into SD microspheres to form a semi-IPN have been attempted. The effect of these modifications was assessed using acoustic sources of pink/white noises and an audio band (4000–5000 Hz). Different internal porous structures of the pristine microspheres cause indistinct divergences of acoustic insulating capabilities in the pink and white noise fields. The surface metallization enhances the reflection and scattering actions but dismantle the viscoelastic absorption feature of polymer bulk. Therefore, metallization on relatively soft MD microsphere could create a better effect than on SD and SDH beads. Embedding soft poly(ethyl acrylate) into individual SD bead demonstrates a clear improvement in the sound proof performance. Additionally, the disk constituted by semi-IPN beads displays a downshift of the panel resonance frequencies relative to the disk made of the corresponding SD beads. © 2006 Wiley Periodicals, Inc. J Appl Polym Sci 102: 1202–1212, 2006

Key words: porous polymer microsphere; acoustic proof medium; semi-IPN; surface-modified particles; metal nanoparticles

INTRODUCTION

The porous polymer matrix is considered as one of the effective sound absorption media with high attenuation coefficients because it contains a large quantity of narrow and tortuous voids and channels. This particular structural feature allows the establishment of a highly extensive temperature-gradient boundary layer because maximum sound pressure amplitude occurs at the surface of the polymer phase.[1,2] Polymer segments located at the polymer–air interface have higher degrees of freedom of motions (in comparison with those packed in the bulk phase) because they feel less constraint of cohesive force, and the loss tangent will as a result be promoted with an increase in the contact area.

This research focuses attention on the sound absorption medium composed of porous polystyrenic microspheres (<50 μm, $\bar{d} = 25$ μm) rather than a continuous and porous medium. From the prospective of real applications, the polymer microsphere is readily being packed in between two suitable reinforced facings to form laminar structure by pressing for achieving sound absorption and reradiation. Recent studies on the acoustic behavior of such porous granular packing have shown that macro- and micro-porosity in the granular exhibits a significant effect on acoustic absorption over a wide range of frequencies.[3–5] The present work pursues structural modifications on polymer microspheres.

The present work started with synthesis of three types of porous polymer microspheres (SD, SDH, and MD), using the suspension polymerization method. A porogen mixture (or diluents) was used in the polymerization system to generate porous structure in each individual bead. The subsequent structural modifications with the aim of tuning its acoustic capacity, and the present work focuses on the following tactics: (1) deposition of Ni nanoparticles on both SD and SDH beads via an *in situ* reduction procedure and on MD beads via electroless nickel (EN) plating; (2) ethyl acrylate (EA) monomer was arranged to undergo polymerization in the surface matrix and pores of SD beads, and as a result, a semi-interpenetrating (IPN) thick shell was generated in each SD bead, described by the symbol SD*x*-EA*y*.

The acoustic shielding capability of the pristine polymer beads and their surface-modified counterparts were studied using pink and white noises and high frequency audio band (4000–5000 Hz) as sound source. Pink noise has equal energy per octave or fractional octave band, perceived by the ear as high and low pitches with equal loudness. Whereas white

Correspondence to: L. Hong (chehongl@nus.edu.sg).

Journal of Applied Polymer Science, Vol. 102, 1202–1212 (2006)

TABLE I
Compositions of the Monomers Feeds and the Divergences Between the Solubility Parameters of Porogen and of Polymer Networks

Symbol	Molar ratio of monomers	Diluents v_{Dec}/v_{Tol}	δ_m (MPa$^{0.5}$)[a]	$\lvert \delta_m - \delta_p \rvert$ (MPa$^{0.5}$)[b]
SD11	ST : DVB = 1 : 1	1 : 1	15.85	2.75
SD31	ST : DVB = 1 : 1	3 : 1	14.68	3.92
SDH11	ST : HEA : DVB = 9 : 1 : 10	1 : 1	15.85	2.95
SDH31	ST : HEA : DVB = 9 : 1 : 10	3 : 1	14.68	4.12
MD12	MA : DVB = 1 : 1	1 : 2	16.63	2.27
MD11	MA : DVB = 1 : 1	1 : 1	15.85	3.05
MD21	MA : DVB = 1 : 1	2 : 1	15.07	3.83

For all reactions, [SDS] = 0.5 wt %; Volume ratio of aqueous to organic = 5 : 1.
[a] Solubility parameter of the porogen, $\delta_m = \delta$ (Dec) × Vol (Dec)% + δ (Tol) × Vol (Tol)%.
[b] Solubility parameters of the respective polymer networks generated: δ_p (SD) = 18.6 MPa$^{0.5}$; δ_p (SDH) = 18.8 MPa$^{0.5}$; δ_p (MD) = 18.9 MPa$^{0.5}$.

noise sounds like the hiss heard when one dials between stations on the radio.

In principle, the high-frequency acoustic absorption of the porous microspherical structure could be improved by tracking the two ways: first, to bolster the reradiation (or scattering) of incident sound waves through raising the surface elastic property. This concept is examined in the present work by forming thin Ni-particle deposition layer on the three types of polymer microspheres; second, to increase the viscoelastic damping capability namely the loss modulus component by bringing into the rigid SD matrix a soft polymer to form the semi-IPN. Both efforts have come out with the responses expected and there is a room for further expanding the modification effects.

EXPERIMENTAL

Materials

Technical grade divinylbenzene (DVB, consisting of *m*-DVB 55.8%, *p*-DVB 24.6% and 3-, 4-ethylvinylbenzene 18.9%, Fluka), styrene (ST, 99%, Aldrich), ethyl acrylate (EA, 99%, Fluka), methyl acrylate (MA, 99%, Fluka), and 2-hydroxyethyl acrylate (HEA, 97%, Fluka) were used after removing inhibitors. Benzoyl peroxide (BPO, moistened with 25% water, Merck), 1,1′-azobis (cyclohexanecarbonitrile) (98%, Aldrich), tetrahydrofuran (THF, 99.99%, Fisher Scientific), and sodium dodecyl sulfate (SDS, 98%, Fluka) were used as received without further purification. Other reagents used for nanonickel deposition via EN plating were of analytical grade.

Synthesis of porous crosslinked microspheres

Porous microspheres of poly(styrene-*co*-divinylbenzene) (SD) were synthesized by the suspension polymerization (molar ratio ST : DVB = 1 : 1), using BPO as the initiator and SDS as dispersant dissolving in the aqueous phase. A mixture of toluene (Tol) and decane was employed as the porogen and diluents with the volume fraction of 0.5 in the monomer feed for generation of porous matrix within microspheres. The synthesis was carried out in a three-necked round bottom flask equipped with a mechanical stirrer, a reflux condenser, and a thermocouple. The mixture was stirred at 600 rpm, to give a suspension of oil droplets dispersed in aqueous phase, under argon gas purging. A three-ramp temperature profile (76°C/3 h, 85°C/3 h, 90°C/5 h) was implemented to conduct the polymerization to guarantee a nominal 50% crosslinking degree. After polymerization, the resultant SD powders were washed with hot THF in Soxhlet extractor for 24 h and then in warm water. Finally, the powder was vacuum dried at 60°C.

Applying the similar procedure, poly(styrene-*co*-2-hydroxyethylacrylate-*co*-divinylbenzene) (SDH) and poly(methyl acrylate-*co*-divinylbenzene) (MD) with the same crosslinking degree was prepared. Basic reactions conditions to construct the above two types of spherical networks are summarized in Table I.

Metallization of polymer microspheres

By means of *in situ* reduction

The SD powder of size < 50 μm (2 g) was soaked in a methanol solution of nickel sulfate (0.5 Ni wt % with respect to the polymer) for 6 h to allow sufficient infiltrating of Ni ions into the porous matrix. Followed by slow evaporation of methanol, the resultant dry powder was dispersed in an alkaline mixture containing hydrazine as reducing agent and PVA as surfactant (Table II). An excess of sodium

TABLE II
The Recipe Used to Reduce Ni^{2+} Salt Trapped Inside SD Beads

Chemicals	Concentrations
Sodium hydroxide (4*M*)	200 mL L^{-1}
Hydrazine ($N_2H_4.H_2O$) 35%	100 mL L^{-1}
Polyvinyl alcohol	5 g L^{-1}
Sodium chloride	50 g L^{-1}

TABLE III
Composition of the EN Plating Solution Formulated in House

Chemicals	Concentrations
Nickel sulfate hexahydrate ($NiSO_4.6H_2O$)	27 g L^{-1}
Sodium phosphinate monohydrate ($NaH_2PO_2.H_2O$)	28 g L^{-1}
Lactic acid ($CH_3CH(OH)CO_2H$)	25 mL L^{-1}
DL-Malic acid (99%) ($HO_2CCH_2CH(OH)CO_2H$)	15 g L^{-1}

pH 4.8; plating temperature: 70°C; EN bath stabilizers: Pb^{2+} ions.

chloride was required to prevent the redissolution of nickel sulfate into the aqueous phase. The *in situ* reduction of Ni^{2+} ions was completed at 80°C for 12 h. The nickel-deposited SD beads were then washed several times in DI water and followed in acetone. They were then placed in a vacuum drying chamber to remove all volatile residues.

By means of electroless plating

The MD powder was activated and sensitized using a colloidal solution of palladium chloride and stannous chloride. After filtration and drying, the sensitized beads (0.5 g) were introduced into the plating solution (50 mL) whose composition is listed in Table III and the EN plating took place forthwith. The duration of plating (10 min) was fixed for all samples, and the plating was manipulated at 70°C, which is about 20°C lower than the required normally for achieving a light plating extent. After this, the plated beads were then washed several times in DI water. The nickel loading was defined as the mass percentage of Ni-P alloy deposited with respect to the total mass of the plated MD.

Embedding linear poly(ethyl acrylate) into the matrix of SD beads

The incorporation of linear poly(ethyl acrylate) into the matrix of SD beads was undertaken by two steps: monomer loading and *in situ* polymerization. For a typical run, the SD11 powder (5 g) were dispersed and stirred in a 50-mL solution of toluene (Tol), EA, and initiator 1,1′-azobis(cyclyhexanecarbonitrile). The volume fraction of EA is 50 vol %, and the concentration of initiator was kept at 1 mol % of EA. After 24-h stirring, the EA-loaded beads were separated from the immersion solution by filtration and redispersed in a 100-mL PVA aqueous solution. The suspension was heated at 80°C for 48 h for *in situ* polymerization of EA inside the matrix of beads. After polymerization, the resultant powder was washed in hot water for several times, followed by Soxhlet extraction with methanol for another 24 h to remove unpolymerized EA from the beads. Finally, the powder was vacuum dried at 50°C for overnight before use. The result of embedding (Table IV) was confirmed by mass increase, porosimetry, and IR spectroscopy. The IR spectrum displays two new peaks at 1750–1735 cm^{-1} and 1300–1030 cm^{-1}, corresponding to the C=O and C—O stretching vibrations of the ester functional group, respectively.

TABLE IV
The Mass Gained Due to Introduction of PEA into the SD Matrix

Symbol	Pore volume and mean radius of SD beads[a]		PEA loading (PEA mass/total mass) × 100%
SD11EA50	0.5936 (mL/g)	104 Å	22.14
SD31EA50	0.7596 (mL/g)	117 Å	27.97

[a] Determined by mercury porosimetry studies.

Characterization of the porous structures by mercury intrusion porosimetry

The porous properties of the three types of microspheres, SD, SDH, and MD were measured on a mercury porosimeter (Micromeritics 9420). At lower intrusion pressure, the tiny microspheres are compressed into a solid mass with roughly constant packing density, provided the disturbance within the penetrometer is minimized under long enough equilibration time. Upon the arrival of breakthrough pressure,[6] at which the interparticle void filling completes, the interstice space registers in mercury porosimetry as pore volume. The pore-volumes inside the microspheres are smaller than the interstice among particles and can be detected at a higher pressure range ~500–60,000 psia.

The surface morphology of different types of microspheres was recorded on a JEOL JSM-5600LV scanning electron microscopy (SEM) instrument. For finer porous structures, their images were taken on

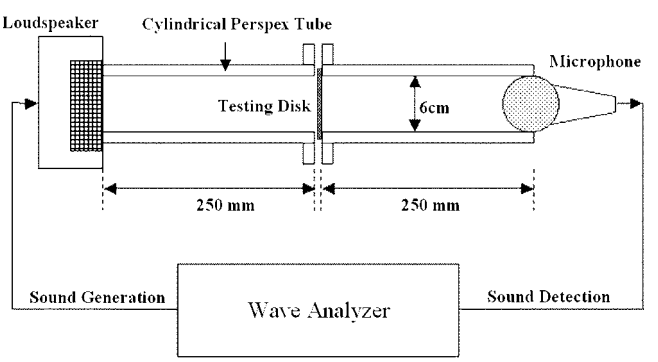

Figure 1 Experiment setup for undertaking the sound attenuation study.

TABLE V
Mercury Intrusion Porosimetry Results

	SD11	SD31	SDH11	SDH31	SD11-EA50	SD31-EA50	MD21	MD11	MD12
Pore volume (mL/g)	0.59	0.76	0.68	0.76	0.15	0.27	0.62	0.79	1.04
Pore area (m^2/g)	113.70	130.15	127.23	122.82	38.21	30.12	145.08	146.20	170.59
Avg pore radius (Å)	104	117	106	124	77	177	86	108	122
Interstitice size (Å)	316	327	288	218	313	320	281	315	331
Porosity (%)	64.12	67.20	61.89	68.64	53.08	56.44	68.14	68.98	72.29

JEOL JSM-6700 field emission scanning electron microscope (FE-SEM).

Differential scanning calorimetry study

DSC analysis of both SD and SD-EA samples were performed on a differential scanning calorimeter (Mettler Toledo) instrument under dry nitrogen atmosphere. The temperature program was designed in such a way that the scan started from −40°C to 180°C and cooled down to −40°C, then the second scan was executed again to 180°C at the constant rate of 10 K min^{-1}. The thermogram of the second heating in the range from −30 to 150°C was recorded.

Sound attenuation study

The measurement of sound attenuation of the powders was performed in a cylindrical attenuation kit made by Perspex tube (Fig. 1). Prerecorded white noise and pink noise were selected as the model incidence wave to carry out the test. A round disk made of the powders (from SD, SDH, MD, and SD-EA series, respectively) was placed at the mid position of the tube. The detected sound intensity was used to evaluate the extent of attenuation by computing the sound transmission loss (TL):[2,7]

$$TL = I_{\text{Attenuated}}/I_{\text{Incidence}} \quad (1)$$

For the preparation of a testing disk ($d = 3$ cm), a given amount of powder was introduced into a solution of methylcellulose (5% by weight of the powder) in water/acetone (v/v = 1 : 2). The resulting paste was thickened quickly by evaporating the solvent under mechanical stirring, and finally a dry powder was obtained. After that, the powder was pressed in a pellet-die on a Carver® hydraulic press (model no. 3912) to the level (0.28 ton/cm^2) for all samples. The thickness of the disks is constantly 2 mm for the amount of powder used. Stationary sinusoidal acoustic waves with frequency range of 4000–5000 Hz with fixed intensity were selected to evaluate the frequency-dependent TL property of the samples.

RESULTS AND DISCUSSION

Mercury intrusion porosimetry

With regarding porosimetry of both SD and SDH series (Table V), it appears that the pore volume, the average pore radius, and porosity increase with increasing decane content in the diluents used in the polymerization system (Table I). Decreasing the volume ratio in the binary diluents mixture (decane/Tol) caused a rougher SD matrix (Fig. 2) and larger pore sizes (Fig. 3), this was attributed to the expanding of the difference in solubility parameter between the diluents and the SD net-

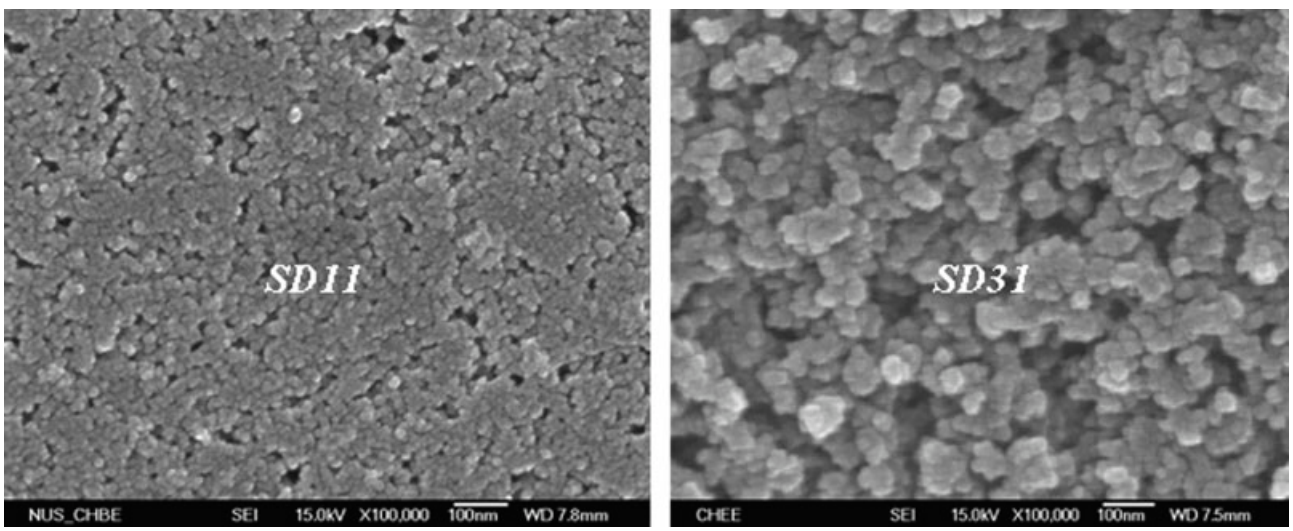

Figure 2 FE-SEM micrographs of the microspheres surface morphology of pristine SD11 and SD31.

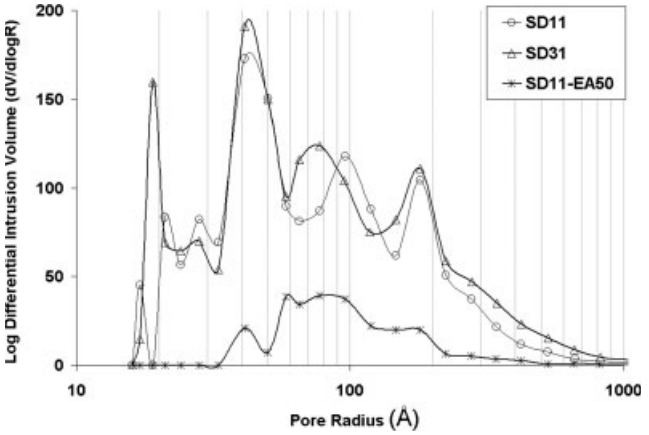

Figure 3 Logarithm different intrusion curves of SD series obtained from the mercury porosimetry analysis.

work $|\delta_m - \delta_p|$ as listed in Table I. The smaller $|\delta_m - \delta_p|$ gave rise to higher solvating power, and hence a less rough matrix and more uniformly distributed pore sizes. Similar trend were found in the MD series. The

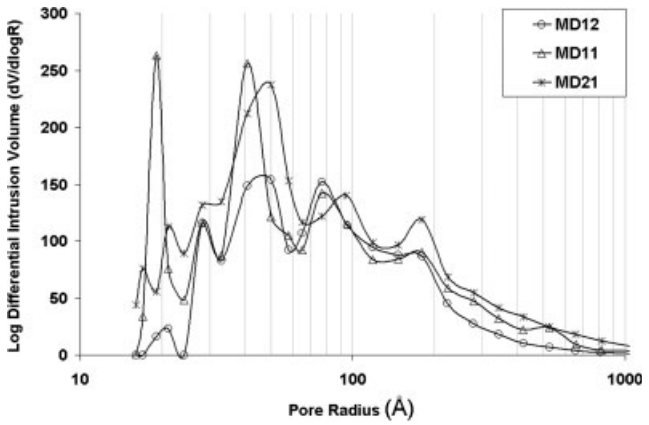

Figure 4 Logarithm different intrusion curves of MD series obtained from the mercury porosimetry analysis.

effects of diluents and the mechanism of formation of porous structures have been studied and reviewed in numerous publications.[8–10]

The diluents system used in the synthesis of SD and MD series produced mesoporous materials (IUPAC classification, mesopores have radii in the range 10–250 Å). Typically, the pore size distribution curves plotted in log differential intrusion volume against pore radius are shown in Figures 3 and 4. As shown, for SD series, both samples exhibit broad pore size distributions falling well in the mesoporous regime prominently from 15 to 200 Å, where various peaks emerge. Increasing the decane content (SD31) shifted the pore distribution curve slightly toward larger pore size, especially for the segment of 150–1000 Å, prompting the formation of macropores. Similar distribution profiles were also generated in the MD series, in which the right shifting of the MD21 curve was due to the decrease in solvating power.

The incorporation of linear EA polymer into SD beads was to embed the soft EA phase in the rigid SD network. A clear drop in the pore area and pore volume that is showed in Figure 3 indicates that such modification design has been realized. The decrease is found to be proportional to the amount of EA loadings. For the higher PEA content (22.14%) as shown in SD11-EA50, the pore size distribution profile is flattened, due to the insertion of poly(ethyl acrylate), which reduce drastically the pore volume of the SD11 matrix. Substantial amount of bulkier PEA linear chains are capable of blocking the pore radius of less than 30 Å during the polymerization process.

Effects of Ni nanoparticles on polymer microspheres

Metallic Ni grains generated via *in situ* reduction as detailed earlier (see By Means of *In-situ* Reduction

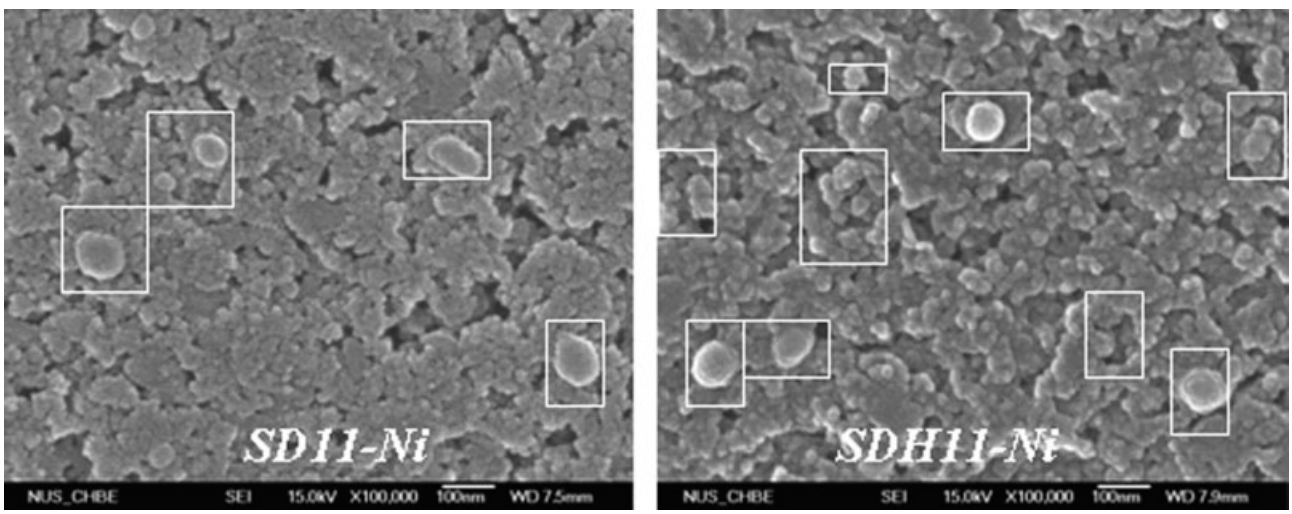

Figure 5 The surface morphologies change after metallization by *in situ* reduction.

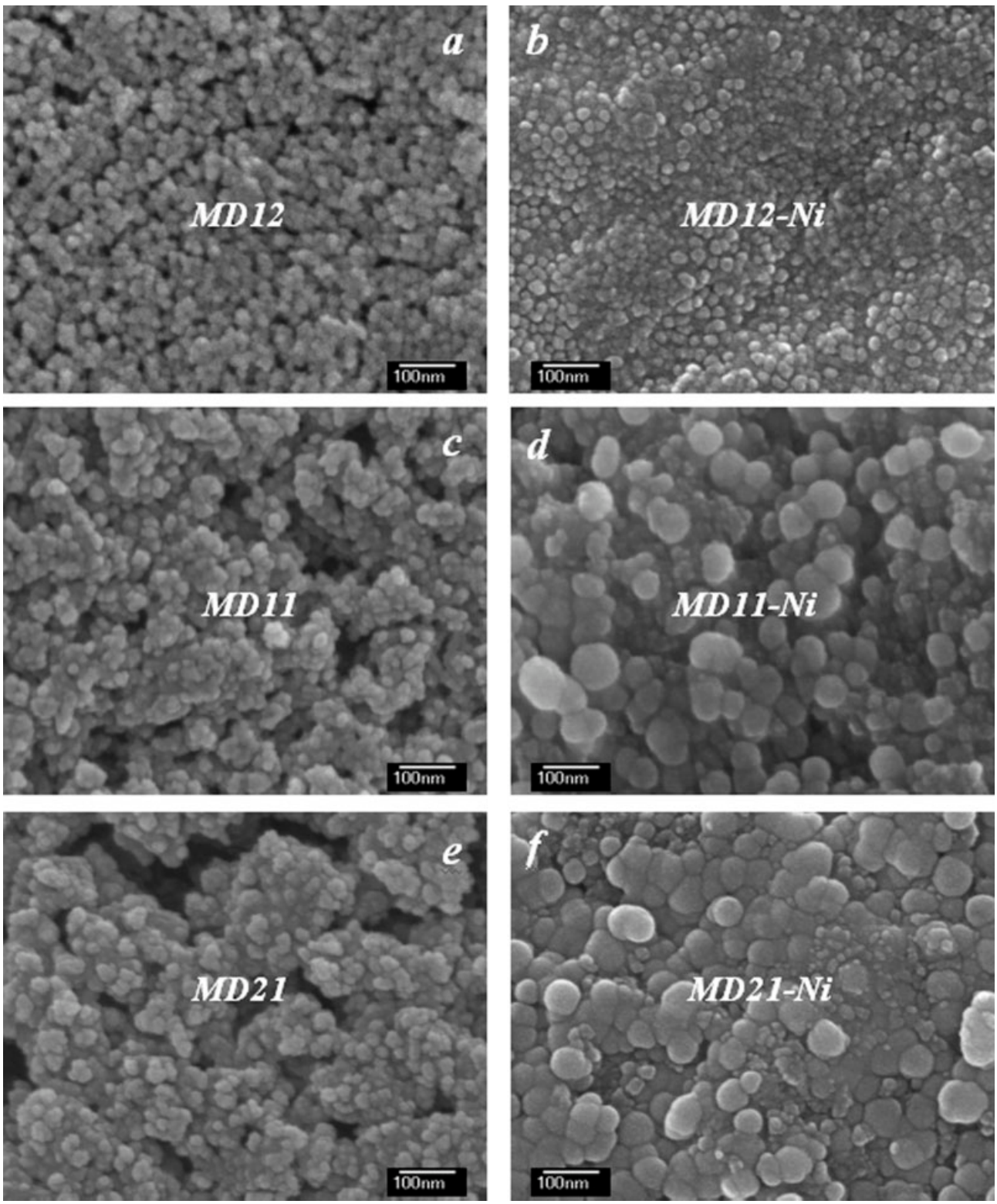

Figure 6 FE-SEM micrographs of the microsphere surface morphology (a, c, e) Pristine MD series; (b, d, f) EN plated counterparts at ×100,000 magnification. (The average Ni-P loading for MD12, MD11, and MD21 was found to be 12.2, 16.4, and 6.1 wt %, respectively.)

section) have the particle size distribution in the range of 30–100 nm. These tiny Ni particles are clutched on the porous surface of SD and SDH particles. It was found that a slightly higher metal distribution density of the Ni nanoparticles could be realized on the surface of SDH beads, where about 10% of composition was constituted by hydrophilic HEA units, in contrast to that of SD beads (Fig. 5).

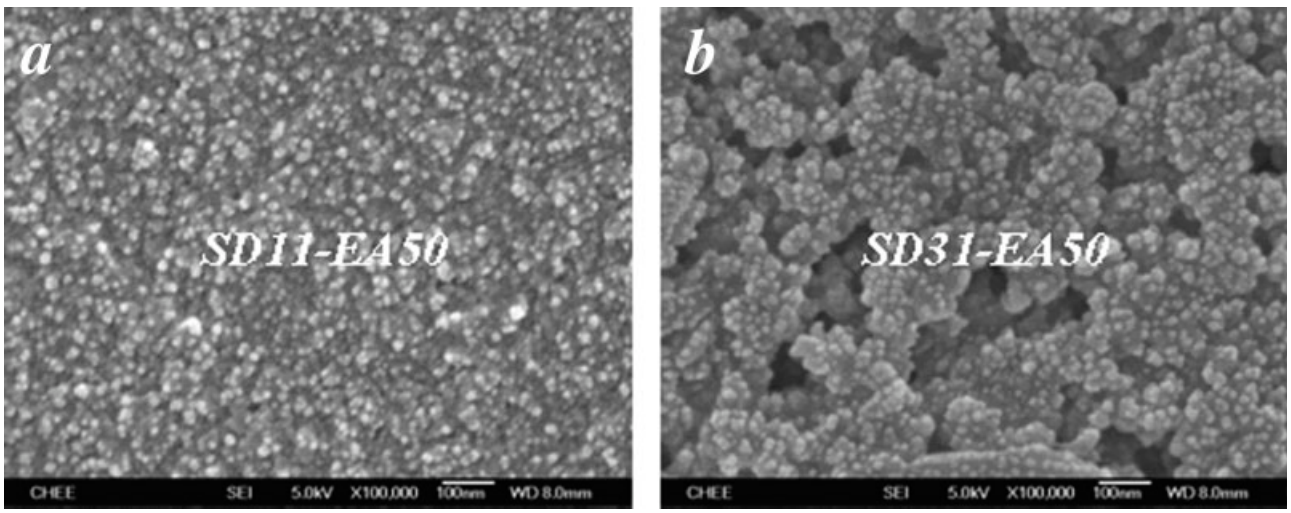

Figure 7 The surface morphologies change after filling of EA polymer.

Hydrophilic modification of the hydrophobic SD surface matrix greatly improves the wetting property of SD beads to the precursor (the alcohol solution of Ni^{2+}) of Ni nanoparticles.

However, the limitation for using *in situ* deposition means is a too low metal loading though it is simple and suits other metals as well. To overcome this limitation, the electroless nickel (EN) plating system shows the advantage only if the plating conditions are deliberately lessened to avoid generation of heavy plating. Following our previous work,[11] we continued with using the MD resin, which contains both rigid and soft blocks linked by chemical bonding, as substrate of EN. The plating gave rise to metallic Ni grains (<50 nm) on MD beads, and smaller Ni particles were found on MD12 than on MD11 and MD21 (Fig. 6). It is quite likely that the growth of Ni particles was constrained on the least porous MD12 surface due to the existence of relatively dilute and segregated seeding sites. On the MD11 surface, the deposition was grown in bunches of 50–100 nm nickel grains. For the case of most porous MD21 surface, the growing of nickel particles were less controllable because of the presence of concentrated seeding sites, which are easier to form on more porous surface during the activation pretreatment for EN plating.

Assessment of sound attenuation

Test of noise TL by pink and white noises

Sound TL is the key parameter to evaluate the porous polymeric insulating medium. The porous polymeric medium attenuates acoustic amplitude relies primarily on three factors: the mass-inertia and elasticity of testing disk, the geometry (pore-size distribution, tortuosity of pore tubes, and roughness of interfacial regions),[2,12] and the viscoelastic properties of the polymer framework.[13–15] The test was carried out using both white and pink noise bands. White

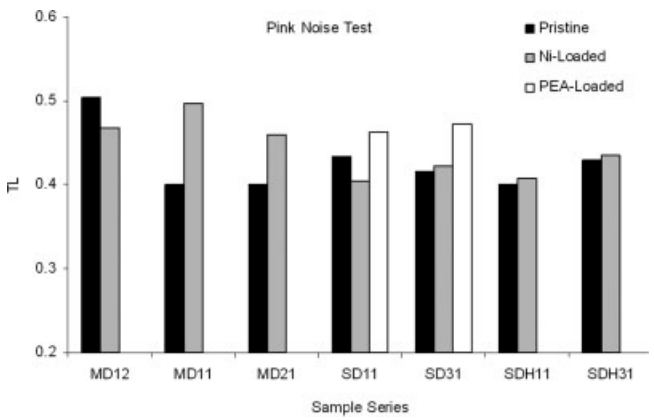

Figure 8 Pink noise transmission loss studies.

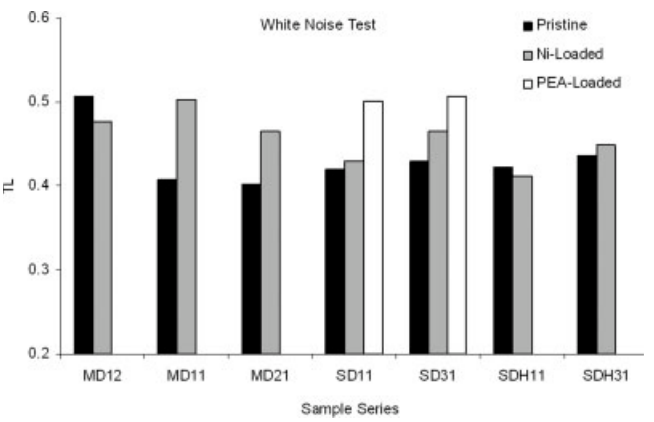

Figure 9 White noise transmission loss studies.

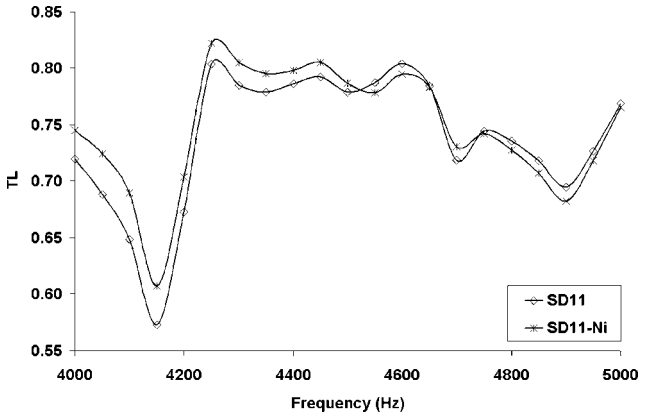

Figure 10 Transmission Loss of SD11 and SD11-Ni in the high frequency range (4000–5000 Hz).

noise is defined as sound with equal intensity per Hz in the audible frequency range. Pink noise is sound with equal intensity per octave (any two sounds whose frequencies make a 2 : 1 ratio are said to be separated by an octave). This tips the energy toward the low frequency; white noise is used for an assessment of loudspeaker sound fields.

Figures 8 and 9 show that the majority of pristine porous beads, i.e., those obtained from the suspension polymerization, possess TL values surrounding 0.4, which is independent of identity and porosity of the absorbent. This is an indication that the inner pores of individual microspheres may involve by a mild way in sound insulation. The interstitial voids (of ~200–300 Å) in the testing disk exert the actual pore flow resistivity, which dissipates the noise via several mechanisms[1,2,12] that all lead to switching part of sound energy into heat. However, among the pristine microspherical resins, MD12 and SD11 displayed higher TL values than the rest. This outcome can be related to their surface porosity, according to Figures 2 and 6, beads of these two resins exhibit relatively denser surface morphologies in contrast to the others. As a result, the surface of these two types of beads possess higher magnitudes of impedance mismatch (defined as the product of mass density and acoustic velocity in the medium of interest), and thus reflection and scattering of sound waves at these two surfaces should be more intense. Both actions convert incident sound waves to a lot of smaller sound wave propagating fields, wherein the destructive interference and net reflection components contribute to raising the TL level of material.

The metallized MD11 and MD21 microspheres show unambiguous improvement in TL level, but they are still below or comparable with the TL of the pristine MD12 (Figs. 8 and 9). On the other hand, for MD12 beads, the deposition of Ni particles on them (Fig. 6) lowered down the TL level oppositely. This outcome implies that in additional to the interfacial attenuation mechanisms (reflection, scattering, mode transfer, and friction),[16,17] attenuation through absorption counts on an appropriate matching between the viscoelastic property of each individual bead (of the testing disk) and frequency of incident sound wave at a given temperature. It is more likely that the presence of a layer of Ni nanoparticles on the three kinds of pristine microspheres enhances the interfacial attenuation mechanisms but weakens the bulk absorption capacity of the beads at the same time. Therefore, the general trend of the variation of TL (under white noise or pink noise test) with metallization shows that relatively heavier Ni deposition is favorable, namely the interfacial mechanisms take the main role in the sound insulation process. Nevertheless, it may note that too thick a Ni layer produces a converse effect according to our previous study.[11]

The pink and white noise test also revealed that incorporating PEA into SD matrix resulted in lifting TL level. On the basis of the changes in SD morphology (Fig. 2 vs. Fig. 7), it can be concluded that embedding

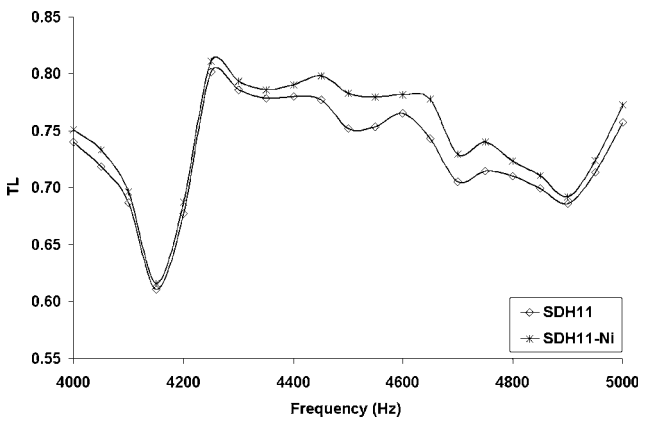

Figure 11 Transmission Loss of SDH11 and SDH11-Ni in the high frequency range (4000–5000 Hz).

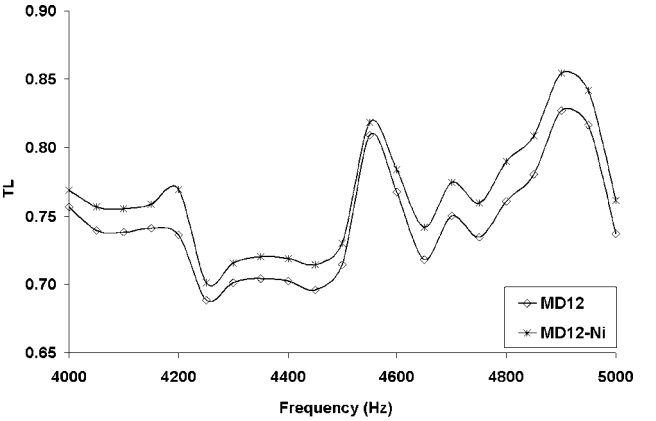

Figure 12 Transmission Loss of MD12 and MD12-Ni in the high frequency range (4000–5000 Hz).

TABLE VI
DSC Results for the Pristine and the PEA-Loaded SD Microspheres

Sample	Transition	T_0 (°C)	T_g (°C)	T_e (°C)	T_g width (°C)	ΔC_p (J g^{-1} K^{-1})
SD11	1	–	–	–	–	–
	2	108.5	112	118	3.5	0.013
SD11-EA50	1	−11	25	50	61	0.093
	2	112.5	124.2	127	14.5	0.031
SD31-EA50	1	−15.5	3.5	32	47.5	0.037
	2	111.5	119.5	121.5	10	0.019

T_0 (onset of glass transition), T_e (ease point of glass transition), and T_g (temperature at which the half of heat capacity is gained).

PEA into SD could benefit not only the interfacial attenuation, as the surface of beads became denser, but also the bulk absorption capability, because PEA is the softer phase in contrast to the rigid SD matrix. The last point that could be drawn (from Figs. 8 and 9) is the relationship between TL of the modified spherical resins and the type of sound source. The modifications made on the MD and SD resin series improve more effectively the TL level of white noise than that of pink noise compared with their pristine counterparts.

Investigation of TL in high frequency range

In this section, the TL properties of the three model microspherical resins (SD11, SDH11, and MD12) were investigated in the relatively high frequency range, 4000–5000 Hz. The metallization of these resins indeed improved to certain extents their sound insulating capability, in particular the Ni-deposited SDH11 and MD12 (Figs. 11 and 12). SDH11-Ni displayed more obvious sound insulating effect than SD11-Ni relative to their respective pristine resins (Figs. 10 and 11), especially in the frequency range from 4500 to 5000 Hz. As known from the above discussion, nano-Ni particles achieved a slightly higher deposition density on SDH beads by virtue of the hydrophilic modification. Therefore, the attenuation actions at particle/air interface of SDH11-Ni were more intense than at that of SD11-Ni. On the other hand, the minor extent of metallization in either case did not alter the TL–*f* (Hz) of the pristine resin. It is quite likely that profile is determined by the panel (or testing disk) properties such as microsphere packing density, interparticle binding, and intrinsic mechanical vibration modes.

The acoustic insulating capability of the testing disk also counts on viscoelastic characteristic of individual microsphere. For instance, the SD11 and SDH11 disks reveal similar the TL–*f* (Hz) profiles because both types of microspheres have very similar frameworks and porous structures (Tables I and V). On the contrary, the MD12 disk shows a higher TL level and different TL–*f* (Hz) profile than the SD11 and SDH11 disks (Fig. 12) over the frequency range of study because it contains 50% by mole of soft poly(methyl acrylate) segments. According to generic frequency dependence of glass transition, the glass-transition temperature (T_g) of PMA segments will increase as the frequency of measurement is increased. Therefore, the loss peak of the PMA at room temperature could happen in a higher frequency range than in that corresponding to its intrinsic T_g (ca.−5°C). Similar to the white/pink noise damping study, the surface metallization of MD12 offers the benefit of raising TL level. It may be also worth to note that the metallization by means of EN plating (on MD series) presents more versatility in sound insulating for white/pink noise tests and the high frequency range evaluation compared with the metallization by *in situ* deposition approach (on SD and SDH series).

Effects of semi-interpenetrating polymer network

Embedding PEA into the SD matrix in effect produces the semi-IPN structure. Compared with the DSC diagram of SD11, the SD11-EA50 powders (Table VI) display an expanded T_g region ($T_e - T_0$) that

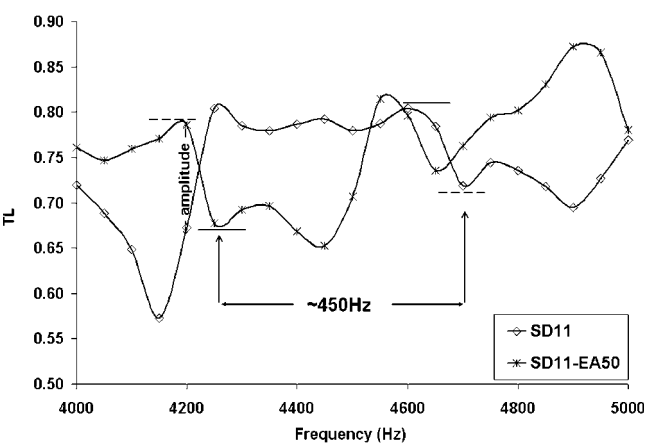

Figure 13 Transmission Loss of SD11 and SD11-EA50 in the high frequency range (4000–5000 Hz).

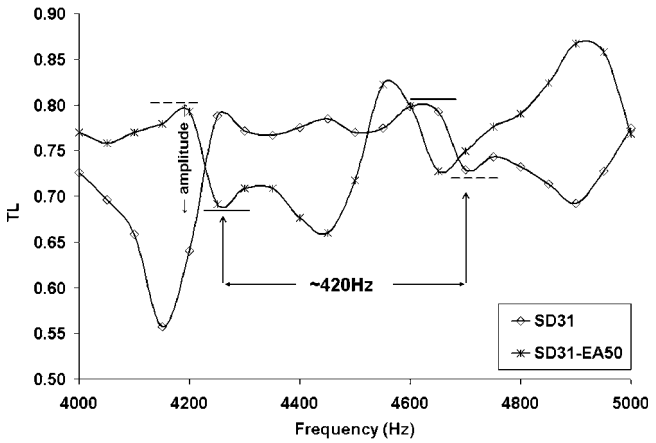

Figure 14 Transmission Loss of SD31 and SD31-EA50 in the high frequency range (4000–5000 Hz).

is known as the glass transition of the styrenic network (row 2) and a new glass transition region (row 1) attributed to the embedded PEA phase (row 1). As reported in literature,[18] the T_g of PEA homopolymer is in the range of -25 to -22°C, nevertheless, this glass-transition range is broadened and extended to the higher temperature direction, which is the indicative of strong interactions of PEA chains with the host network, namely forming the semi-IPN. This became relatively milder in SD31-EA50, where the PEA loading was about 27.97%, according to their glass-transition range. This is because the increase in the loading of PEA in bigger pores (in SD31 beads) would lead to formation of tiny PEA bulk phases that resemble to pristine PEA than those entrapped in SD11 network; hence this part of rubbery PEA tiny phase was responsible to the lowering down of T_g.

It has been known that SD-EA disks showed better sound-proof performance in white noise and pink noise fields than SD disks. Furthermore, the SD-EA disks also exhibit a rather different TL–*f* (Hz) profile from the SD counterparts in the selected frequency range of 4000–5000 Hz (Figs. 13 and 14). Namely, the TL–*f* (Hz) profiles of both SD11-EA and SD31-EA disks were noticeably ahead of the corresponding SD disks by about 420 to 450 Hz and revealed stronger amplitude of resonance peaks. This suggests that the soft PEA phase even though trapped in discrete beads can work collectively to respond punching of sound waves when they are closely packed. In fact, combining the SD and SD-EA curves in either test of Figure 13 or 14 suggests us that a disk assembled by laminas of SD and SD-EA would achieve much better sound proof result than each of them because they form a nice compensation at those frequencies where one of them has low TL level. On the other hand, based on the comparison of sound insulating performance of SD11-EA with SD31-EA or SD11 with SD31 in the testing acoustic frequency range, it could be concluded that difference in EA loading of the former set or in porosity of the later set affects very slightly the performance.

CONCLUSIONS

The porous microspheres of SD series, its modified form poly(2-hydroxyethyl acrylate/styrene-*co*-divinylbenzene) (SDH series) with particle sizes of (<50 μm, $\bar{d} = 25$ μm) and MD series have been synthesized and used as the acoustic materials to evaluate their sound TL properties, based on white or pink noise and audio range of 4000–5000 Hz. The testing disk composed of a particular type of microspheres contains two types of pores: interstices among the packed microspheres and mesopores in each microsphere. On the basis of this structure, the TL is brought about by intrinsic polymer network vibration, intermicrospheres vibration, and the whole disk vibration, of which the elastic component contributes to sound waves reradiation and the viscous component to energy conversion. In the white noise and pink noise studies, the interfacial dissipation was only predominant in interstitial voids. Only the redirection and reflection due to incorporated nickel particles by EN plating in MD matrix can differentiate the acoustic performance of the testing disks. Implantation of nano-sized Ni particles on the SDH matrix improves the attenuation coefficient in the high frequency range; this modification is attributed to the reinforcing of polymer network due to the metal–polymer attractive interaction and therefore, raising the elastic property. Formation of the semi-IPN by weaving in the SD matrix poly(ethyl acrylate) chains reveals the similar high frequency sound insulating effect up to a maximum of 0.8, but it is ascribed to the enhancement of viscous component.

References

1. Allard, J. F. Propagation of Sound in Porous Media, Modeling Sound Absorbing Materials; Elsevier: Essex, UK, 1993; Chapters 4 and 7.
2. Kuttruff, N. Room Acoustics, 4th ed.; Elsevier: New York, 2000; Chapter 6.
3. Voronina, N. N. Appl Acoust 1998, 55, 67.
4. Boutin, B.; Royer, P.; Auriault, J. L. Int J Solids Struct 1998, 35, 4709.
5. Voronina, N. N.; Horoshenkov, K. V. Appl Acoust 2003, 64, 415.
6. Webb, P. A.; Orr, C. Analytical Methods in Fine Particle Technology; Micromeritics Instrument Corporation: Norcross, GA, 1997; Chapter 4.
7. Everest, F. A. The Master Handbook of Acoustics, 4th ed.; McGraw-Hill: New York, 2001; Chapters 2 and 8.
8. Wojaczynska, M.; Kolarz, B. N. J Appl Polym Sci 1995, 56, 433.
9. Erbay, E.; Okay, O. Polym Bull 1998, 41, 379.
10. Okay, O. Prog Polym Sci 2000, 25, 711.

11. Ng, Y.-H.; Hong, L. J Polym Sci Part B: Polym Phys 2004, 42, 2710.
12. Pierce, A. D. Acoustic: An Introduction to its Physical and Application; Acoustical Society of America: New York, 1989.
13. Jones, D. I. G. Handbook of Viscoelastic Vibration Damping; Wiley: Chichester, England; 2001, Chapter 3.
14. Hu, R.; Dimonie, V. L.; El-Aasser, M. S.; Pearson, R. A.; Hiltner, A., Mylonakis, S. G.; Sperling, L. H. J Polym Sci Part B: Polym Phys 1997, 35, 1501.
15. El-Aasser, M. S.; Hu, R.; Dimonie, V. L.; Sperling, L. H. Colloids Surf A 1999, 153, 241.
16. Jarzynski, J. In: Sound and Vibration Damping with Polymers; Corsaro, R. D., Sperling, L. H., Eds.; American Chemical Society: Washington, DC, 1990. ACS Symposium Series, Vol. 424, p 167.
17. Jarzynski, J.; Balizer, E.; Fedderly, J. J.; Lee, G. In: Encyclopedia of Polymer Science and Technology; Mark, H. F., Kroschwitz, J. I., Eds.; Wiley: New York, 2003; Vol. 3.
18. Andrews, R. J.; Grulke, E. A. In Polymer Handbook, 4th ed.; Brandrup, J.; Immergut, E. H.; Grulke, E. A., Eds.; Wiley: New York, 1999; p VI/199.